Direct ink writing of vascularized self-healing cementitious composites

Wan, Zhi; Xu, Yading; He, Shan; Chen, Yu; Xie, Jinbao; Šavija, Branko

DOI
10.1016/j.cemconcomp.2023.105295

Publication date
2023

Document Version
Final published version

Published in
Cement and Concrete Composites

Cement and Concrete Composites 144 (2023) 105295

Contents lists available at ScienceDirect

Cement and Concrete Composites

journal homepage: www.elsevier.com/locate/cemconcomp

Direct ink writing of vascularized self-healing cementitious composites

Zhi Wan *, Yading Xu, Shan He, Yu Chen, Jinbao Xie, Branko Šavija

Microlab, Faculty of Civil Engineering and Geosciences, Delft University of Technology, Delft, the Netherlands

ARTICLE INFO

Keywords:
3D printing
Vascular network
Self-healing
Printing direction

ABSTRACT

Direct ink writing of cementitious materials can be an alternative way for creating vascular self-healing concrete by intentionally incorporating hollow channels in the cementitious matrix. In this study, a 3D-printable fibre reinforced mortar was first developed. Three groups of specimens were fabricated using direct ink writing, where the two top and bottom printing layers were printed with different printing directions. The macrostructure of the hardened specimens was studied using CT scanning. Four-point bending tests were carried out to investigate the initial flexural strength and the strength recovery after healing with injected epoxy resin. Furthermore, water permeability test was used to evaluate the healing potential of the samples. The results from CT scanning show that printing direction influences the actual volumes of hollow channels and the volume of small pores which are a consequence of the deposition process. The hollow channels of all samples were squeezed by the upper layers during the printing process, and the longitudinally printed samples were the most affected. When printing direction changes from longitudinal to transverse, the initial flexural strength decreases. Similarly, the average permeability of the cracked samples increases when the printing direction changes from longitudinal to transverse. Although the healing effectiveness regarding flexural strength is remarkable for all specimens, it was only possible to perform a single healing process as hollow channels were then blocked by the epoxy resin. The rough surface of the hollow channels is inferred to make it difficult to extract the epoxy resin out of the specimens.

1. Introduction

Self-healing concrete has great potential to enhance the durability of concrete structures without significantly increasing the maintenance or repair costs [1,2]. There are three main approaches for self-healing in cementitious materials [3]: autogenous healing, capsule based healing, and vascular healing. Among others, further hydration of the unreacted cement clinker is one of the main mechanisms contributing to the autogenous self-healing in concrete. To promote further hydration, minerals or crystalline admixtures can be directly included in the mix [4–6]. In addition, healing agents could be encapsulated and incorporated in the cementitious matrix, forming capsule based self-healing concrete [7,8]. In addition to inorganic materials, polymers [9–11] and bacteria [12–14] could also be stored in the capsules. Compared with the (stimulated) autogenous healing, the maximum healable crack width is higher for capsule based self-healing concrete [15]. However, the limited amount of healing agent in the capsules significantly hinders sealing larger cracks as well as performing multiple healing processes.

By contrast, the availability of sufficient healing agents enables vascular self-healing cementitious materials to seal wider cracks [16]. Huang et al. [8] demonstrated that vascular self-healing concrete shows a better healing effectiveness than the capsule counterpart when using the same healing agent (i.e., calcium hydroxide solution). However, unlike capsule based self-healing concrete, the healing agents for vascular self-healing cementitious materials are usually liquids such as sodium silicate solution, cyanoacrylate, epoxy resin and others [17]. Except for healing agents, vascular materials play an important role in the healing performance of vascular self-healing cementitious materials. The vascular material needs to be strong enough to withstand the process of concrete mixing and casting, while at the same time being brittle enough to trigger the self-healing process [18]. Glass tubes have been widely used in concrete, acting as vascular networks to transport the healing agents [8,19,20]. Other materials such as cementitious hollow tubes (CHTs) [21,22], starch or inorganic phosphate cement (IPC) [16] have also been investigated. However, the brittle behaviour of vascular materials makes it difficult to create vascular networks with complicated geometry. As a result, one-dimensional (1D) or two-dimensional (2D) vascular networks are ubiquitous in the literature [20,23].

* Corresponding author.
E-mail addresses: Z.Wan-1@tudelft.nl (Z. Wan), Y.Xu-5@tudelft.nl (Y. Xu), S.He-2@tudelft.nl (S. He), Y.Chen-6@tudelft.nl (Y. Chen), J.Xie-1@tudelft.nl (J. Xie), B.Savija@tudelft.nl (B. Šavija).

https://doi.org/10.1016/j.cemconcomp.2023.105295
Received 28 April 2023; Received in revised form 5 September 2023; Accepted 9 September 2023
Available online 11 September 2023

The rapid development of additive manufacturing (AM, also known as 3D printing) is beneficial to vascular self-healing materials because it facilitates the fabrication of complicated vascular networks [24–27]. In cementitious materials, vascular networks are usually additively manufactured using fused filament fabrication (FFF) with thermoplastic materials such as Acrylonitrile Butadiene Styrene (ABS) [16,28,29] and polylactic acid (PLA) [30,31]. Although these thermoplastic filaments allow fabricating vascular networks with complicated geometry, the presence of interface between the vascular and the cementitious matrix may induce ingress of water [28]. Alternatively, hollow channels can be created inside the cementitious matrix and used as pathways for transporting the healing agent. The simplest approach is to form the hollow channels by taking out preplaced bars from the moulds after concrete setting [32,33]. More complicated hollow channels could be found in the work of Sangadji and Schlangen [34], where porous network concrete (PNC) was introduced as a kind of vascular self-healing concrete. Similar to self-healing polymers, sacrificial materials have also been employed to fabricate the hollow channels for cementitious composites [35,36]. Due to its water solubility, polyvinyl alcohol (PVA) filament has been investigated for creating hollow channels. Li et al. [30] studied the dissolution of 3D-printed PVA vascular embedded in the cementitious matrix, considering the highly alkaline environment, showing that it is feasible to create hollow channels using PVA filament considering that the dissolution of PVA is not influenced by the pH of environment. However, PVA reacts with the $Ca(OH)_2$ from the cementitious matrix, causing its expansion and possible matrix cracking. To alleviate this issue, Wan et al. [37] proposed coating the 3D-printed PVA vascular to prevent the reaction with the cementitious matrix. Although the 3D hollow channels were successfully created, the process of fabrication and dissolution of the 3D-printed PVA vascular network is labour-intensive. Furthermore, the 3D-printed vascular is relatively small, making its upscaling to large-scale structures non-trivial.

Compared with stereolithography (SLA) and FFF, direct ink writing (DIW) is an extrusion-based additive manufacturing technique which is capable of printing 3D structure with any ink material holding proper rheological behaviours [38]. As a result, DIW of polymers, ceramics, cement paste, metals and other materials has been previously studied [39]. Direct ink writing of cementitious materials can be an alternative way for creating vascular self-healing concrete [40–43]. For self-healing concrete, hollow channels could be intentionally incorporated in the cementitious structures to act as the 'vascular network'. However, to the best of the authors' knowledge, there have been no attempts to achieving this. In direct ink writing of cementitious materials, printing direction tends to influence the printing quality as well as the interlayer bond [44]. More importantly, the reserved hollow channels may be squeezed during the printing process. As a result, the actual volume of the hollow channels may be different when different printing directions are used.

In this study, fibre reinforced mortar with hollow channels is additively manufactured as vascular self-healing cementitious material. First, a 3D-printable fibre reinforced mortar was designed as the printing ink. Prisms with 3D hollow channels were printed with three printing directions (longitudinal, inclined and transverse). The printed samples were examined using X-Ray computed tomography (CT scanning) after hardening to investigate the influence of printing direction on the structures of hollow channels. The flexural strengths under 4-point bending of the virgin samples were tested. Furthermore, a water permeability test was carried out on the cracked samples. Afterwards, epoxy resin was injected as the healing agent to heal the cracked samples. The healing performance regarding the flexural strength regain and the water permeability is compared and discussed.

2. Materials and methods

2.1. Materials and setups

2.1.1. Mix design of a 3D printable mortar

Herein, a mix design of the 3D-printable mortar presented. The material for 3D printing needs to have good pumpability and buildability [45]. A low water/cement ratio should ensure the stiffness and the strength of the extruded materials for good buildability [46]. However, low water/cement ratio could cause problems for the pumpability of the materials. Therefore, superplasticizer (Glenium 51) is added to improve the fluidity of the cementitious material. Besides, hydroxypropyl methylcellulose-based viscosity modifying admixture (VMA) is added to improve the cohesion and consistency of the fresh mixture [47,48]. After a series of trial-and-error tests, the water/cement ratio is determined as 0.343.

To avoid brittle failure of specimens during mechanical tests, ultra-high molecular weight polyethylene fibre (UHMWPE) is incorporated into the cementitious matrix to enhance the ductility. However, it has been shown that a large percentage of fibres may introduce air voids and fibre balls during the printing process [49]. Based on our previous research [37], 0.17 vol% of PE fibre is added to the printing mix. The mix design of the 3D printable mortar is given in Table 1.

An Anton Paar MCR 302e rheometer was used to determine the flow properties of the proposed mixture [50]. For each measurement, 85–90 g of fresh paste was filled into the measuring cup. Note that time zero is defined as the moment when water is added to the dry components during mixing. After a pre-shear ($60s^{-1}$ of shear rate and 30s of duration time) and resting session (30s), the flow curve test was executed at the material age of 5 min. The shear rate ramped linearly from $0s^{-1}$–$30s^{-1}$ within 1 min and was maintained at $30s^{-1}$ for 40s. After that, the shear rate was decreased in four consecutive steps from $30s^{-1}$–$10s^{-1}$ and was kept constant at about 40 s for each step. The data was recorded each 0.2s. A detailed test protocol is presented in Fig. 1(a). For each shear rate regime in the descending part, the shear stress was averaged by using the final 50 measuring points. The flow curve is shown in Fig. 1(b). For the fresh cementitious materials, the Herschel-Bulkley (HB) model (Equation (1)) is often used to describe the rheological behaviour [51]. Note that the model is identical to Bingham model when the exponent is 1.

$$\tau = \tau_0^{'} + k\dot{\gamma}^n \tag{1}$$

Where $\tau_0^{'}$ is the dynamic yield stress; k and n are consistency factor and power index, respectively.

After the flow curve test and 5min of resting, a constant shear rate (CSR) test was conducted to measure the static yield stress at the material age of 15 min. In CSR test, the applied shear rate was $0.1s^{-1}$ and testing time was 40s. This test was also performed at material age of 30, 45 and 60 min. The resting time between two tests was about 14 min. As shown in Fig. 1(c), the peak value of shear stress in CSR test could be seen as static yield stress (SYS) [52].

As shown in Fig. 1(a), the shear stress-shear rate curve could be well fitted with the Herschel-Bulkley model. For this mixture, the value of $\tau_0^{'}$, k and n are 1235.38, 0.3555 and 2 respectively. Since the fitted component is 2, the designed mortar cannot be employed in a printing process with a high shear/extrusion because the shear thickening behaviour would make the apparent viscosity become too high for the mix to be pump and extruded. The static yield stress of the mix can be

Table 1
Mix design of the 3D printable mortar (kg/m^3).

Cement IIIB 42.5	water	Sand (0.125–0.25 mm)	Superplasticizer (Glenium 51)	VMA	UHMWPE
1385.1	474.7	117.0	0.28	1.1	1.7

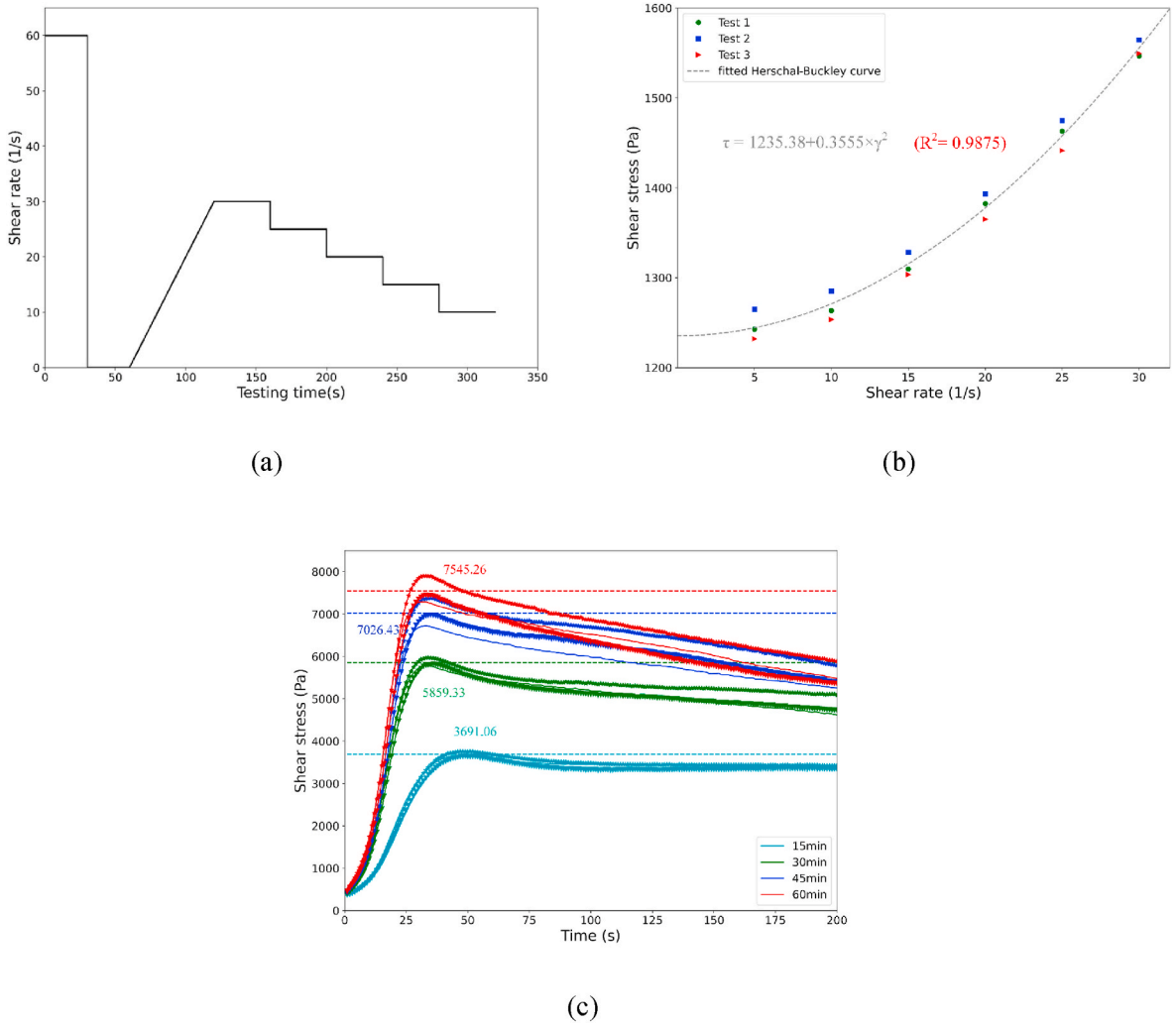

Fig. 1. (a) Testing protocol of flow curve; (b) Flow curve; (c) Shear stress under constant shear rate.

found in Fig. 1(c). While the static yield stress increases with time, the speed of increase gradually decreases.

2.1.2. Design of the vascular network

For simplicity, rectangular cross sections are used to form the networks. The joint angle of the second and third generation of vascular network are chosen as 90° (Fig. 2).

As shown in Fig. 2(a), for ease of printing, the first and second generation of vascular network have the same height. Furthermore, the width of the second and third generation of vascular are identical. Although the cross section is rectangular, one side length in each generation of vascular network is designed based on Murray's law (Equation (2)) to minimize the flow energy of the healing agents [53]. Considering that the diameter of the nozzle is chosen as 4 mm in this study, the height of third generation of vascular network is set as 4 mm (See Fig. 2(a)). Based on Equation (2), the widths of second and first generation of vascular networks are calculated as 5.04 mm and 6.36 mm respectively. The length and width of the printed mortar are designed as 200 mm and 50 mm respectively due to the restraint of printing table (480 mm (length) × 480 mm (width) × 500 mm (height)). The height is set as 32.5 mm and the details could be found in Section 2.1.3. Note that the positions of vasculature measured from the printing bed (bottom

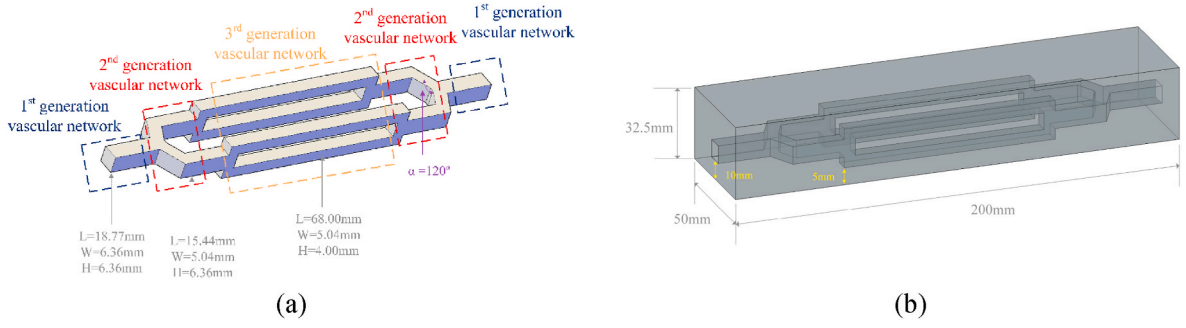

Fig. 2. Schematic of the 3D-printed mortar with hollow channels. (a) Vascular network; (b) Mortar with vascular networks.

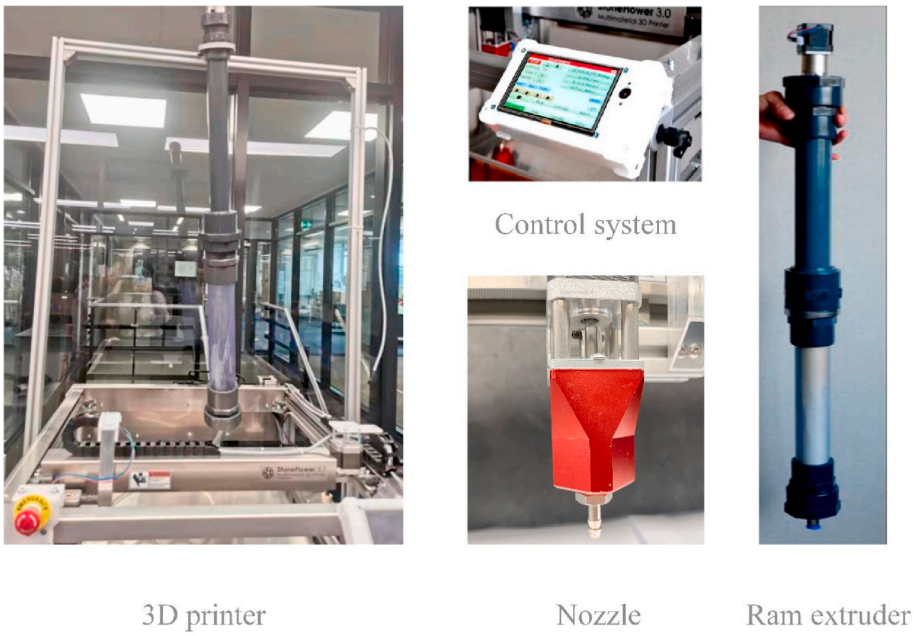

Fig. 3. The Stone Flower 3.1 Multi-material 3D printer and its components.

vascular: 5 mm; middle vascular: 10 mm; upper vascular: 17.5 mm) are chosen in accordance with the printing layer-height (2.5 mm). This is described in more detail in Fig. 4. The volumes of the designed cementitious matrix and hollow channels (i.e., vascular network) are calculated as 302.18 cm^3 and 22.82 cm^3, respectively. The 3D model is designed using Auto CAD, and the slicing is carried out with Matlab software. The actual volumes of matrix and hollow channels with different printing directions will be calculated based on the CT scanning results in Section 3.1.

$$\sum r_p^3 = \sum r_d^3 \tag{2}$$

where r_p and r_d are the radii of the parent vessel and the daughter vessel, respectively.

2.1.3. *Printing process*

In this study, an extrusion-based commercial 3D printer (Stone Flower 3.1 Multi-material 3D printer) was used for printing (see Fig. 3). As shown in Fig. 3, a ram extruder, consisting of electrical machinery, a steel bar and a piston, is fixed on a gantry. The prepared printing material is stored in the cylinder with a maximum volume of 1.5 L [46]. After the printing file is imported to the 3D printer, operations could be performed through the touch screen of the control system. During the printing process, all relevant information (printing time, printing speed …) is displayed on the screen. The diameter of the nozzle is chosen as 4 mm in this study. The selection of nozzle diameter is mainly based on laboratory trial tests, rather than rheological tests (section 2.1.1.), which are used for material characterization. For the used 3D printer, nozzles with three different diameters are available, i.e., 2.5 mm, 4.0 mm and 6.0 mm. It was tested to be difficult to extrude the designed mortar using the 2.5 mm nozzle. One of the possible reasons is that the fibre length is

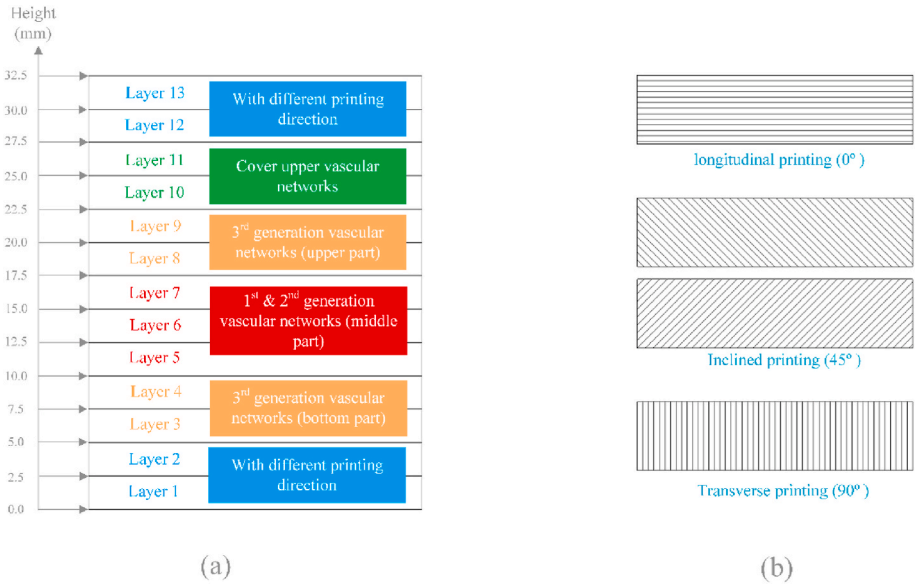

Fig. 4. Schematic description of (a) Printing layers and (b) printing direction.

6 mm, which is much larger than the nozzle diameter. On the other hand, to ensure the printing accuracy of samples, a relatively small nozzle is preferred. Therefore, we decided to print with the smaller of the two remaining nozzles, i.e., the 4.0 mm one. The rotor above the nozzle helps remove the bubbles from the printing materials before extrusion.

Before the printing process, the fibre reinforced mortar is mixed as follows: (1) The dry components (cement, sand and VMA) were pre-mixed in a Hobert mixer for 4min; (2) Water and superplasticizer were added to the dry components and mixed for 4min; (3) Fibres were added and mixed for 4min. The mixed mortar was then filled in the cylinder of 3D printer.

It has been shown that the mechanical behaviour of 3D-printed materials is influenced by printing direction [44]. To investigate the influence of printing directions, different variants have been used for the bottom and top 2 printing layers: longitudinal (0°), inclined (45°) and transverse (90°); the remaining layers have been transversely printed to minimize the cantilevered length of the layers above the hollow channels. The schematics of different paths are shown in Fig. 4. As shown in Fig. 4(a), two layers without the vascular network (i.e., Layer 10 and 11) have been printed to cover the vascular networks before printing the top two layers (Layer 12 and 13). Therefore, there are 13 layers in the height direction. Since the printing layer-height is set as 2.5 mm, the height of the sample is 32.5 mm. The printing speed is set as 10 mm/s, and the movement speed is set as 20 mm/s when changing the printing layer in the height direction. The inflow velocity of mortar is 60 cm/min and it takes approximately 45min for the entire printing process.

After determining the printing parameters, one specimen was first printed to test the pumpability and buildability of the mix design (Fig. 5). From Fig. 5, it is obvious that the designed mortar is suitable for 3D printing since the printing quality of the samples is remarkable with very limited visible imperfection between the interlayers.

2.1.4. Curing and healing process

After the printing process, the samples were kept on the printing table for 24 h covered with plastic film to mitigate water evaporation. Afterwards, the hardened specimens were moved to a curing room where the relative humidity (RH) and temperature are kept as 96% ± 2% and 20 ± 2 °C, respectively. They were cured for 28 days before the first round of mechanical testing. The mechanical properties of the printed samples at 28 days will be compared with the cast counterparts in future research.

After the mechanical test, the cracked samples were injected with a two-component epoxy resin (Conpox Resin BY 158 and Conpox Hardener BY 2996 supplied by Condor Kemi A/S). According to Refs. [28,34], epoxy resin shows a remarkable healing performance as the healing agent. We have used the same healing process in our previous work: (i) Epoxy resin is manually injected into the cracked samples through one inlet while the other inlet is blocked with clip; (ii) Pressurized air is injected to blow the extra epoxy resin out of the hollow channels for the reuse of hollow channels after 30min [37]. The amount of epoxy resin is kept as 30 ml considering the volume of designed hollow channels (22.82 ml). The injected samples were kept in room temperature for 24 h until the next round of mechanical tests.

2.2. Characterization methods

2.2.1. CT scanning

A CT scanner (TESCAN CoreTOM) was used to observe the influence of the printing direction on the printing quality of the samples before the mechanical tests. The voltage and power are set as 140 kV and 40 W respectively. The resolution of the scanned slice is 75 μm. The actual volumes of cementitious matrix, hollow channels and small pores are compared and discussed. The structures were reconstructed using the Dragonfly software. Median filter is employed before segmentation. One specimen was scanned for each designed printing parameter.

2.2.2. 4-Point bending test

The fracture behaviour of virgin samples printed in different directions was studied using a servo press (INSTRON 8872). These specimens were loaded with a constant crack opening speed of 0.5 μm/s until the crack width reached 450 μm [13]. Considering that the crack is

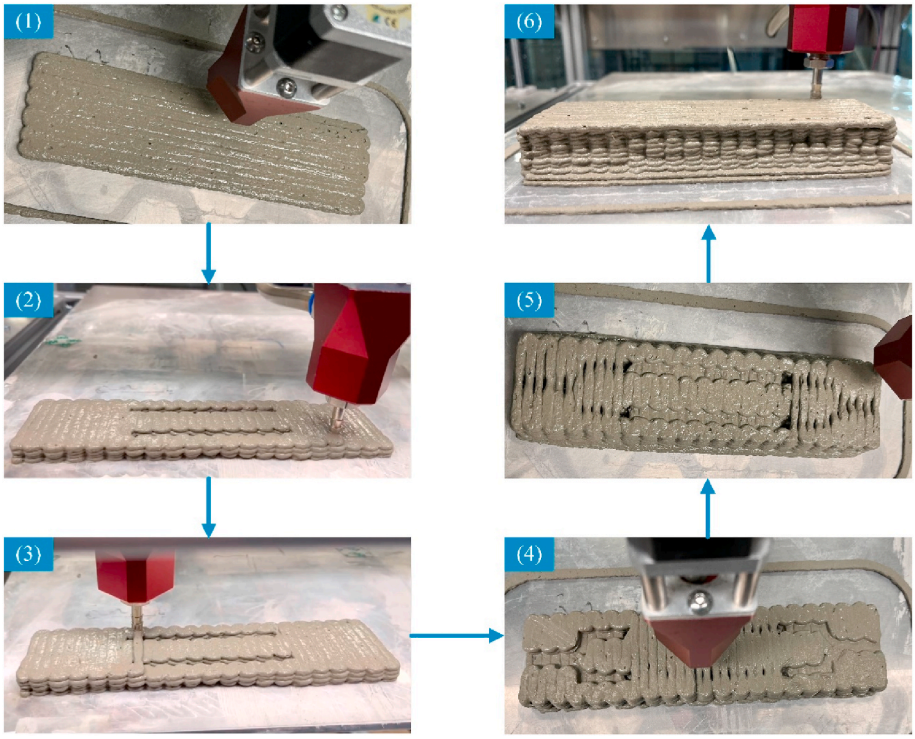

Fig. 5. Printing process of mortar with hollow channels as vascular networks (longitudinal printing path).

likely to develop in the weak inter-layer of the printed samples, there is only one crack during the 4-point bending test. The change of crack width was monitored with a Linear Variable Differential Transformer (LVDT) on the bottom surface of the samples. In this study, the LVDTs go across the whole midsection of the specimen (i.e., between the loading points), where the cracks will surely occur. The crack width was recorded until the samples were totally unloaded. The 4-point bending test is shown schematically in Fig. 6. There are two specimens in each group.

For the healed samples, another 4-point bending test was carried out to evaluate the mechanical response of the samples after injecting the healing agent (epoxy resin). The healed samples were reloaded to 500 μm with a crack opening speed of 0.5 μm/s.

2.2.3. Water permeability test

The water uptake test is widely used to evaluate the watertightness recovery in self-healing cementitious materials [54]. However, considering the defects of the 3D printed specimens and the rough surface, it may be inaccurate to assess the watertightness recovery using water uptake in our case. Instead, an equipment with constant water level is employed for water permeability test. Water permeability of the cracked samples was measured and compared. On one hand, the water permeability of the samples before and after healing can be used to evaluate the sealing efficacy in terms of watertightness [13]. In addition, the water permeability of the cracked specimens could reflect the healing capacity of the samples: the cracked specimens with larger permeability tend to have greater self-healing potentials compared with the ones with smaller permeability in that the higher permeability allows more healing agents to enter the cracks [37]. In particular, one end of the hollow channels was blocked with a clip while the other end was connected to a tube, which was connected to a water container whose height is 0.75 m from the upper surface of the specimens. The water tightness was measured by calculating the flowing speed of the leaked water.

3. Results and discussion

3.1. Macrostructure of samples with different printing directions

3.1.1. Influence of printing direction on the hollow channels

As mentioned above, the reserved hollow channels would be squeezed by the upper printing layer during the printing process. The influence of printing direction on the actual volumes of cementitious matrix and hollow channels is investigated and the reconstructed CT results are shown in Fig. 7.

As shown in Fig. 7, the shapes of actual hollow channels are different from the designed one. Instead of the rectangular cross section in each generation of the vascular network, the hollow channels are irregular, which is caused by two reasons: (1) The hollow channels are squeezed by the self-weight of the layers above; and (2) the imperfections occurring between the printed layers induce additional hollow channels. There are more additional hollow channels in the transversely printed sample than in the other cases. A possible reason is that the interlayers are aligned from bottom layer to top layer, so the interlayers are always in the same places. Compared with transversely and inclined printed specimens, the hollow channels of the longitudinally printed sample are less continuous, which may influence the transport of healing agents during the healing process. To quantitatively investigate the influence of printing direction on the vascular network, the ratios between actual and designed volume of matrix and hollow channels are given in Fig. 8.

The actual volumes of hollow channels in the three groups decrease by more than 40% of the designed hollow channel (Fig. 8). When the printing direction changes from longitudinal (0°) to transverse (90°), the volume of cementitious matrix and hollow channels show a decrease and an increase, respectively. Although the printing direction influences the actual volume of hollow channels, the printable material should be further optimized in order to achieve better buildability and mitigate the squeezing of hollow channels from the upper layers.

3.1.2. Influence of printing direction on the pores

Compared with the cast samples, 3D-printed samples have higher porosity due to the layer-by-layer printing process [55]. Therefore, the influence of printing direction on the porosity is also investigated by comparing the volume of small pores (i.e., those that occur purely as a consequence of the printing process) (Fig. 9). Note that the pores connected to the designed hollow channels are regarded as part of the 'vascular network' in this study.

Additional small pores are present in all specimens (Fig. 9). Compared with the inclined- and longitudinally printed samples, there are more additional pores in the transversely printed one. The total volumes of additional pores are calculated based on CT scanning (Fig. 10). Note that only pores larger than the XCT resolution are considered.

The volume of small pores increases when the printing direction changes from longitudinal (0°) to transverse (90°) (Fig. 10). From Fig. 8, it is found that the volume of cementitious matrix in longitudinally printed specimens is larger than the other two groups. As a result, the larger self-weight load of upper layers squeezes not only the hollow channels, but also the small pores.

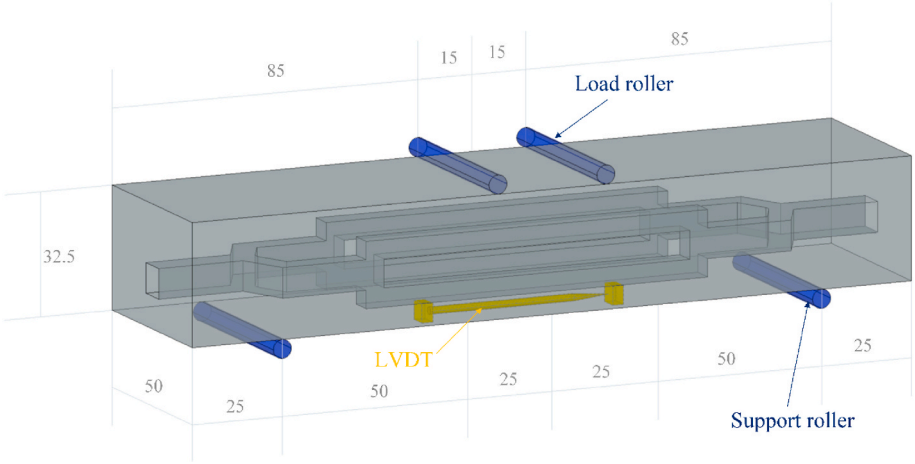

Fig. 6. Schematic of 4-point bending test.

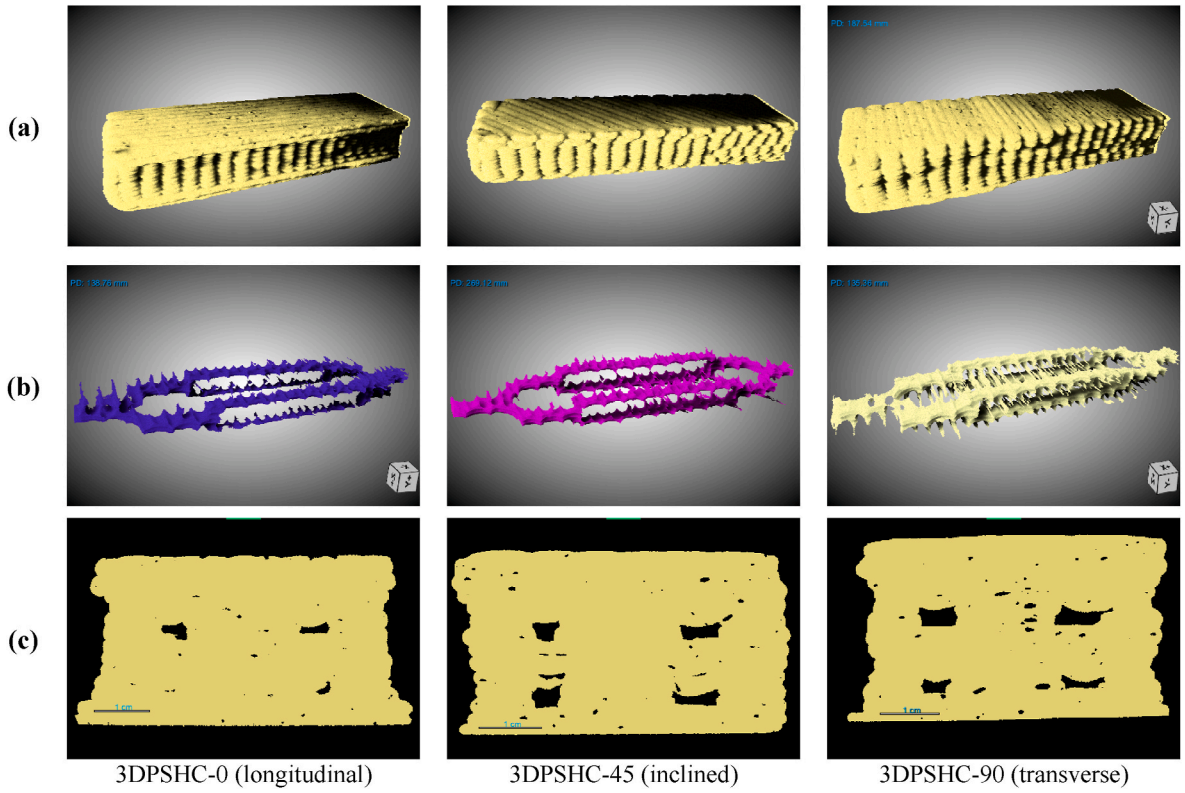

Fig. 7. Reconstructed CT scan results of 3D-printed mortar with hollow channels. (a) The scanned whole samples; (b) The reconstructed hollow channels; (c) Cross sections in the middle part (yellow: matrix; black: hollow channels or small pores). (For interpretation of the references to colour in this figure legend, the reader is referred to the Web version of this article).

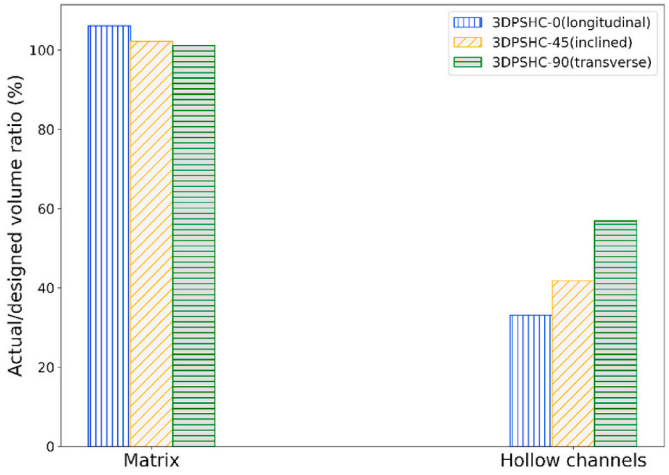

Fig. 8. Reconstructed CT scan results of 3D-printed mortar with hollow channels.

3.2. Fracture behaviour

3.2.1. Initial flexural stress

The facture behaviour of the virgin samples is first investigated through 4-point bending test. The stress-crack width curves of specimens printed in 3 different directions are shown Fig. 11.

Flexure stress/crack width curves are significantly influenced by the printing direction (Fig. 11). The flexural strength of the longitudinally printed specimens is higher than those of the inclined printed and transversely printed specimens (see Fig. 12(b)). According to section 3.1, the possible reasons are the denser cementitious matrix (less pores) and the smaller volume hollow channels in the longitudinally printed specimens. Except for flexural strength, the stiffness of longitudinally- and inclined printed specimens is clearly higher than the transversely printed counterpart.

Different post-peak behaviour is also observed for the three groups. Although the interlayers of transversely-printed samples are parallel to the loading direction, the transversely-printed samples still show ductile behaviours. This could be a result of fibres bridging the cracks. In other words, crack do not always occur in the interlayers. The flexural stress when unloading at the crack width of 450 μm is defined as the residual flexural stress. However, the ductility of transversely- and inclined printed samples is higher than the transverse one due to the higher residual flexural stress. Compared with the transversely printed samples, there are more fibres bridging the cracks. This could also be verified by the larger crack closure of the inclined and longitudinally printed samples after unloading.

3.2.2. Flexural strength of the healed samples

After the first round of 4-point bending test, epoxy resin was injected to seal the cracks. Another round of 4-point bending was carried out on the healed samples. Based on [21,28], the healing performance could be estimated with healing efficiency (Equation (3)) and load recovery index (Equation (4)). The result is shown in Fig. 12

$$\eta = p^{healed} / p^{original} \times 100\% \tag{3}$$

where p^{healed} and $p^{original}$ are the healed fracture load and the original fracture load, respectively.

$$LRI = \frac{P_r - P_u}{P_p - P_u} \times 100\% \tag{4}$$

where LRI represents the load recovery index; P_p and P_r are the maximum load of the virgin and healed samples, respectively; P_u is the

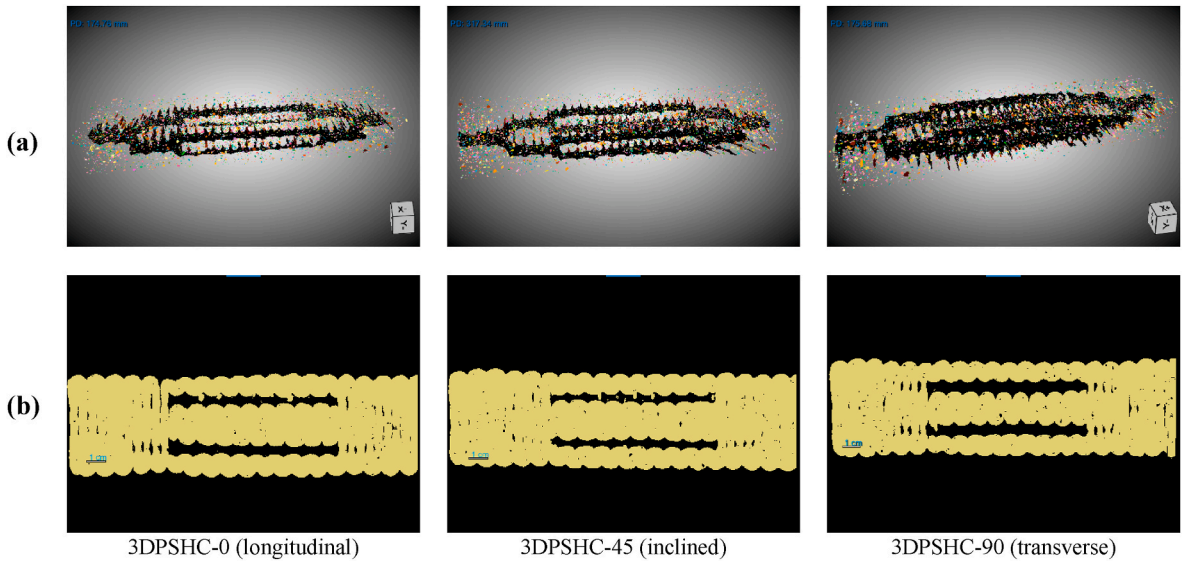

Fig. 9. Sliced CT results of 3D-printed mortar with hollow channels. (a) Reconstructed hollow channels and pores (black: hollow channels; colourful: small pores); (b) Vertical sections (yellow: matrix; black: hollow channels or small pores). (For interpretation of the references to colour in this figure legend, the reader is referred to the Web version of this article).

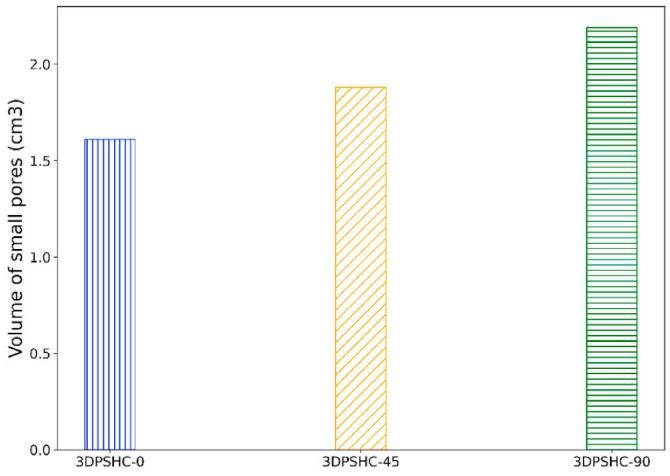

Fig. 10. Volume of small pores of specimens printed in different direction.

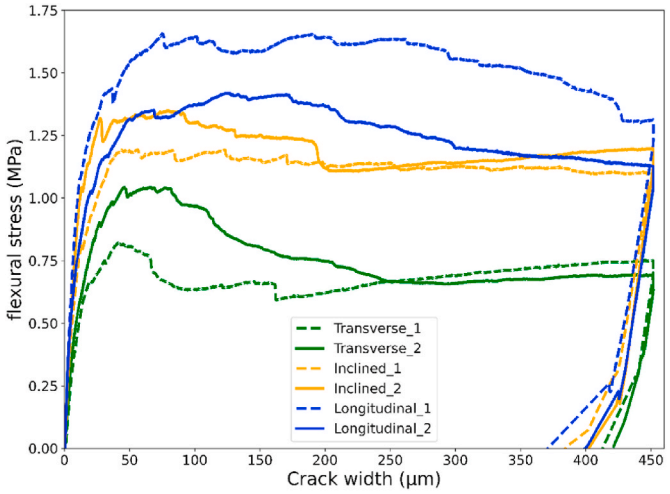

Fig. 11. Flexural response comparison of specimens printed with different directions.

residual load of the virgin samples after unloading.

All specimens regain flexural strengths after the healing process (Fig. 12(a)). Similar to our previous research [56], the residual load-bearing capacity of the healed samples increases compared with the original ones. In particular, the residual flexural stress of inclined and longitudinally printed specimens is much higher than the transverse one. The change of flexural strength can be seen in Fig. 12(b). The average flexural strength of longitudinally printed samples is the largest amongst the three groups. Compared with the other two groups, there are less defects in the longitudinally printed samples. As a result, most of the injected epoxy resin flows into the crack thereby sealing it. However, except for filling the crack, the injected epoxy resin may also fill the printing defects since enough epoxy resin (30 ml) was supplied during the healing process. As a result, the healing efficiency of transversely printed samples is also remarkable. Note that the variance in transversely printed samples is larger than in the other two groups.

As to the influence of printing direction on healing performance, it is found that the healing efficiency and load recovery index of three groups show the same trend (see Fig. 12(c)). The overall self-healing performance of the 3D-printed samples improves when the printing direction changes from longitudinal to transverse. However, compared with healing efficiency, the change of load recovery index is more obvious due to the relatively low initial flexural strength of transversely printed samples. Furthermore, the variance of load recovery index of transversely printed sample is extremely large compared with other two groups.

3.3. Water permeability test

Except for flexural stress, the water permeability of the cracked samples is also investigated. The water permeability of the cracked samples before injecting epoxy resin is shown in Fig. 13.

Based on Fig. 13, the permeability of cracked samples is also influenced by printing direction. When the printing direction changes from longitudinal to transverse, the average permeability of the samples increases. There are two reasons for the increase of permeability. On the one hand, the printing defects increase when the printing direction changes (see Fig. 10). On the other hand, from Fig. 11, the final crack width (i.e., after unloading) decreases when printing direction changes from longitudinal to transverse. Therefore, the average permeability of transversely printed specimens is larger than that of the longitudinally

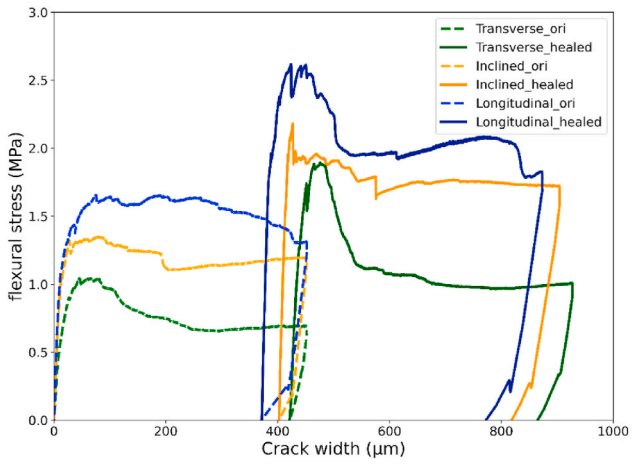

(a)

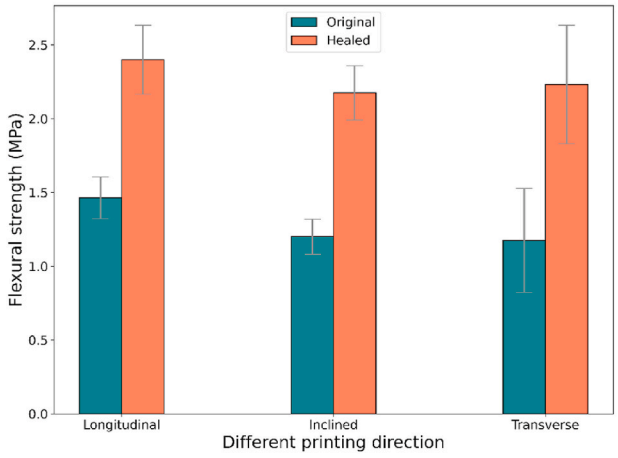

(b)

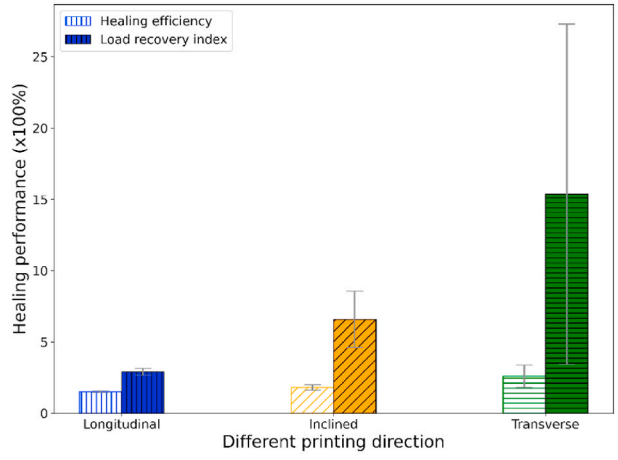

(c)

Fig. 12. (a) Flexural stress-crack width curve after healing; (b) Flexural strength comparison of healed samples printed in different directions; (c) Healing performance of sample printed in different directions.

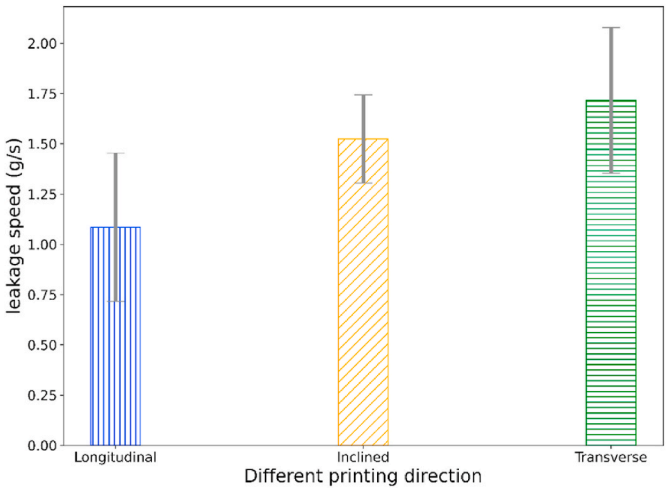

Fig. 13. Flow speed of leaked water of specimens printed in different directions.

printed ones. It is worth mentioning that the variance of the permeability is very large for all of the three groups. This is probably caused by the variability in the printing quality which inevitably exists even when the printing direction is the same.

As to the water permeability of the healed specimens, no leaked water was observed for all the samples. Besides, epoxy resin could not be injected through either of the two outlets. Therefore, it is hard to evaluate the water tightness recovery in this study. It is inferred that the hardened epoxy resin blocks the hollow channels although pressurized air was blown to remove the extra epoxy in the hollow channels. The rough surface of the hollow channels (see Fig. 7(b)) makes it difficult to blow the epoxy resin out of the specimens. More importantly, the squeezing from the upper layers allows for the hollow channels be easily blocked with the epoxy resin. In order to perform multiple healing events with the 3D-printed mortar with hollow channels, the squeezing to the hollow channels should be addressed from the aspect of printable materials. Furthermore, squeezing of hollow channels during the printing process should be considered when designing the vascular system in the future study.

4. Conclusions

In this study, vascular self-healing cementitious material is directly ink written by reserving hollow channels in the cementitious matrix as the path for healing agent transportation. The rheology of the designed fibre reinforced mortar was first investigated. Afterwards, vascular self-healing cementitious materials were fabricated, where the top and bottom two printing layers were printed in three different directions (i.e., longitudinal, inclined and transverse). The influence of printing direction on the macrostructure of 3D-printed specimens was investigated through CT scanning. Furthermore, 4-point bending tests were performed to assess the flexural strength as well as the flexural strength regain after injecting epoxy resin as the healing agent. The water tightness of the cracked specimens printed in different directions was also measured. Based on the results, the following conclusions could be drawn:

(1) The actual volumes of hollow channels are much smaller than the designed volume, with more than 40% of the hollow channels being squeezed by the upper layers during the printing process. The actual amount of "squeezing" depends on the printing direction. The volume of small pores is also influenced by printing direction: it increases when the printing direction changes from longitudinal to transverse. Although printing direction influences

the actual volume of hollow channels, the printable material should be further optimized in order to achieve better buildability and mitigate the squeezing of hollow channels from the upper layers.

(2) The flexural strength of 3D-printed samples is influenced by the printing direction. The longitudinally printed specimen has the highest initial flexural strength amongst the three groups, followed by inclined printed specimens. The residual stress of longitudinally printed specimens is also the highest. A possible reason is that more fibres bridge the cracks in longitudinally printed samples.

(3) The flexural strength regain of the three groups is remarkable since all of the samples have the healing effectiveness of over 100%. The average flexural strength of longitudinally printed samples is the largest amongst the three groups. However, only one healing process could be carried out due to the blockage of hollow channels. The rough surface of the hollow channels makes it difficult to blow the epoxy resin out of the specimens. Except for improving the printing materials, squeezing of hollow channels during the printing process should be considered when designing the vascular system to enable multiple healing events in the future study.

(4) When the printing direction changes from longitudinal to transverse, the average water permeability of the samples before healing increases. The water tightness recovery after the healing process is unknown due to the blockage of hollow channels.

Declaration of competing interest

The authors declare that they have no known competing financial interests or personal relationships that could have appeared to influence the work reported in this paper.

Data availability

Data will be made available on request.

Acknowledgement

Zhi Wan and Jinbao Xie would like to acknowledge the financial support of the China Scholarship Council (CSC) under the grant agreement No.201906220205 and No. 202006260045. Shan He acknowledges the financial supports from the MSCA-ITN project SMARTINCS. This project has received funding from the European Union's Horizon 2020 research and innovation programme under the Marie Skłodowska-Curie grant agreement No 860006. Yading Xu and Branko Šavija acknowledge the financial support of the European Research Council (ERC) within the framework of the ERC Starting Grant Project "Auxetic Cementitious Composites by 3D printing (ACC-3D)", Grant Agreement Number 101041342. Views and opinions expressed are however those of the author(s) only and do not necessarily reflect those of the European Union or the European Research Council. Neither the European Union nor the granting authority can be held responsible for them. The authors would like to acknowledge Mr. Arjan Thijssen for the support in CT scanning tests.

References

[1] D. Rooij, M. R, E. Schlange, "Self-healing Phenomena in Cement-Based materials." Draft of State-Of-The-Art Report of RILEM Technical Committee 221-SHC, 2011.
[2] V. Cappellesso, D. di Summa, P. Pourhaji, N. Prabhu Kannikachalam, K. Dabral, L. Ferrara, et al., A review of the efficiency of self-healing concrete technologies for durable and sustainable concrete under realistic conditions, Int. Mater. Rev. (2023) 1–48, https://doi.org/10.1080/09506608.2022.2145747.
[3] K. Van Tittelboom, N. De Belie, Self-healing in cementitious materials-a review, Materials 6 (2013) 2182–2217, https://doi.org/10.3390/ma6062182.
[4] L. Ferrara, V. Krelani, F. Moretti, On the use of crystalline admixtures in cement based construction materials: from porosity reducers to promoters of self healing, Smart Mater. Struct. 25 (2016), 084002, https://doi.org/10.1088/0964-1726/25/8/084002.
[5] H. Huang, G. Ye, D. Damidot, Effect of blast furnace slag on self-healing of microcracks in cementitious materials, Cement Concr. Res. 60 (2014) 68–82, https://doi.org/10.1016/J.CEMCONRES.2014.03.010.
[6] Z. Zhou, Z. Li, D. Xu, J. Yu, Influence of slag and fly ash on the self-healing ability of concrete, Trans Tech Publications Ltd, Adv. Mater. Res. 306–307 (2011), https://doi.org/10.4028/www.scientific.net/AMR.306-307.1020, 1020–3.
[7] R. Alghamri, A. Kanellopoulos, C. Litina, A. Al-Tabbaa, Preparation and polymeric encapsulation of powder mineral pellets for self-healing cement based materials, Construct. Build. Mater. 186 (2018) 247–262, https://doi.org/10.1016/j.conbuildmat.2018.07.128.
[8] H. Huang, G. Ye, Z. Shui, Feasibility of self-healing in cementitious materials - by using capsules or a vascular system? Construct. Build. Mater. 63 (2014) 108–118, https://doi.org/10.1016/j.conbuildmat.2014.04.028.
[9] B. Dong, G. Fang, Y. Wang, Y. Liu, S. Hong, J. Zhang, et al., Performance recovery concerning the permeability of concrete by means of a microcapsule based self-healing system, Cem. Concr. Compos. 78 (2017) 84–96, https://doi.org/10.1016/j.cemconcomp.2016.12.005.
[10] A. Kanellopoulos, P. Giannaros, D. Palmer, A. Kerr, A. Al-Tabbaa, Polymeric microcapsules with switchable mechanical properties for self-healing concrete: synthesis, characterisation and proof of concept, Smart Mater. Struct. 26 (2017), 045025, https://doi.org/10.1088/1361-665X/aa516c.
[11] C. Xue, W. Li, J. Li, V.W.Y. Tam, G. Ye, A review study on encapsulation-based self-healing for cementitious materials, Struct. Concr. 20 (2019) 198–212, https://doi.org/10.1002/SUCO.201800177.
[12] E. Tziviloglou, Z. Pan, H.M. Jonkers, E. Schlangen, Bio-based self-healing mortar: an experimental and numerical study, J. Adv. Concr. Technol. 15 (2017) 536–543, https://doi.org/10.3151/jact.15.536.
[13] E. Tziviloglou, V. Wiktor, H.M. Jonkers, E. Schlangen, Bacteria-based self-healing concrete to increase liquid tightness of cracks, Construct. Build. Mater. 122 (2016) 118–125, https://doi.org/10.1016/j.conbuildmat.2016.06.080.
[14] Á. González, A. Parraguez, L. Corvalán, N. Correa, J. Castro, C. Stuckrath, et al., Evaluation of Portland and Pozzolanic cement on the self-healing of mortars with calcium lactate and bacteria, Construct. Build. Mater. 257 (2020), 119558, https://doi.org/10.1016/j.conbuildmat.2020.119558.
[15] N De Belie, E. Gruyaert, A. Al-Tabbaa, P. Antonaci, C. Baera, D. Bajare, et al., A review of self-healing concrete for damage management of structures, Adv. Mater. Interfac. 5 (2018), 1800074, https://doi.org/10.1002/ADMI.201800074.
[16] P. Minnebo, G. Thierens, G. De Valck, K. Van Tittelboom, N De Belie, D. Van Hemelrijck, et al., A novel design of autonomously healed concrete: towards a vascular healing network, Materials 10 (2017) 49, https://doi.org/10.3390/ma10010049.
[17] Y. Shields, T. Van Mullem, N. De Belie, K. Van Tittelboom, An investigation of suitable healing agents for vascular-based self-healing in cementitious materials, Sustain. Times 13 (2021) 12948, https://doi.org/10.3390/SU132312948, 2021; 13:12948.
[18] D. Snoeck, N. De Belie, Repeated autogenous healing in strain-hardening cementitious composites by using superabsorbent polymers, J. Mater. Civ. Eng. 28 (2016) 1–11, https://doi.org/10.1061/(asce)mt.1943-5533.0001360.
[19] C. Joseph, A.D. Jefferson, B. Isaacs, R. Lark, D. Gardner, Experimental investigation of adhesive-based self-healing of cementitious materials, Mag. Concr. Res. 62 (2010) 831–843, https://doi.org/10.1680/macr.2010.62.11.831.
[20] K. Van Tittelboom, N. De Belie, D. Van Loo, P. Jacobs, Self-healing efficiency of cementitious materials containing tubular capsules filled with healing agent, Cem. Concr. Compos. 33 (2011) 497–505, https://doi.org/10.1016/j.cemconcomp.2011.01.004.
[21] A. Formia, S. Irico, F. Bertola, F. Canonico, P. Antonaci, N.M. Pugno, et al., Experimental analysis of self-healing cement-based materials incorporating extruded cementitious hollow tubes, J. Intell. Mater. Syst. Struct. 27 (2016) 2633–2652, https://doi.org/10.1177/1045389X16635847.
[22] A. Formia, S. Terranova, P. Antonaci, N. Pugno, J. Tulliani, Setup of extruded cementitious hollow tubes as containing/releasing devices in self-healing systems, Materials 8 (2015) 1897–1923, https://doi.org/10.3390/ma8041897.
[23] D. Gardner, A. Jefferson, A. Hoffman, R. Lark, Simulation of the capillary flow of an autonomic healing agent in discrete cracks in cementitious materials, Cement Concr. Res. 58 (2014) 35–44, https://doi.org/10.1016/j.cemconres.2014.01.005.
[24] C.J. Hansen, W. Wu, K.S. Toohey, N.R. Sottos, S.R. White, J.A. Lewis, Self-healing materials with interpenetrating microvascular networks, Adv. Mater. 21 (2009) 4143–4147, https://doi.org/10.1002/ADMA.200900588.
[25] A.R. Hamilton, N.R. Sottos, S.R. White, Self-healing of internal damage in synthetic vascular materials, Adv. Mater. 22 (2010) 5159–5163, https://doi.org/10.1002/adma.201002561.

[26] J.F. Patrick, K.R. Hart, B.P. Krull, C.E. Diesendruck, J.S. Moore, S.R. White, et al., Continuous self-healing life cycle in vascularized structural composites, Adv. Mater. 26 (2014) 4302–4308, https://doi.org/10.1002/adma.201400248.
[27] K.S. Toohey, N.R. Sottos, J.A. Lewis, J.S. Moore, S.R. White, Self-healing materials with microvascular networks, Nat. Mater. 6 (2007) 581–585, https://doi.org/10.1038/nmat1934.
[28] Z. Wan, Y. Xu, Y. Zhang, S. He, B. Šavija, Mechanical properties and healing efficiency of 3D-printed ABS vascular based self-healing cementitious composite: experiments and modelling, Eng. Fract. Mech. 267 (2022), 108471, https://doi.org/10.1016/J.ENGFRACMECH.2022.108471.
[29] Y. Shields, N.M. Alderete, P Van Den Heede, Y.V. Zaccardi, Influence of 3D Printed Vascular Networks in Self-Healing Cementitious Materials on Water Absorption Studied via Neutron Imaging, 2022.
[30] Z. Li, LR de Souza, C. Litina, A.E. Markaki, A. Al-Tabbaa, Feasibility of using 3D printed polyvinyl alcohol (PVA) for creating self-healing vascular tunnels in cement system, Materials 12 (2019) 3872, https://doi.org/10.3390/ma12233872.
[31] E. Tsangouri, C. Van Loo, Y. Shields, N. De Belie, K. Van Tittelboom, D.G. Aggelis, Reservoir-vascular tubes network for self-healing concrete: performance analysis by acoustic emission, digital image correlation and ultrasound velocity, Appl. Sci. 12 (2022), https://doi.org/10.3390/app12104821.
[32] S. Pareek, A. Oohira, A fundamental study on regain of flexural strength of mortars by using a self-repair network system, in: Proc. 3rd Int. Conf. Self Heal. Mater., Bath, UK, vol. 2729, 2011.
[33] Z. Wan, Z. Chang, Y. Xu, B. Šavija, Optimization of vascular structure of self-healing concrete using deep neural network (DNN), Construct. Build. Mater. 364 (2023), 129955, https://doi.org/10.1016/J.CONBUILDMAT.2022.129955.
[34] S. Sangadji, E. Schlangen, Self healing of concrete structures - novel approach using porous network concrete, J. Adv. Concr. Technol. 10 (2012) 185–194, https://doi.org/10.3151/jact.10.185.
[35] R.E. Davies, A. Jefferson, R. Lark, D. Gardner, A Novel 2D Vascular Network in Cementitious Materials, 2015.
[36] R. Davies, T. Jefferson, D. Gardner, Development and Testing of Vascular Networks for Self-Healing Cementitious Materials, 2021, https://doi.org/10.1061/(ASCE)MT.1943-5533.0003802.
[37] Z. Wan, Y. Zhang, Y. Xu, B. Savija, Self-healing cementitious composites with a hollow vascular network created using 3D-printed sacrificial templates, Eng. Struct. 289 (2023), 116282, https://doi.org/10.1016/J.ENGSTRUCT.2023.116282.
[38] T.V. Neumann, M.D. Dickey, Liquid metal direct write and 3D printing: a review, Adv. Mater. Technol. 5 (2020), 2000070, https://doi.org/10.1002/ADMT.202000070.
[39] M.A.S.R. Saadi, A. Maguire, N.T. Pottackal, M.S.H. Thakur, M.M. Ikram, A.J. Hart, et al., Direct ink writing: a 3D printing technology for diverse materials, Adv. Mater. 34 (2022) 1–57, https://doi.org/10.1002/adma.202108855.
[40] S. Bhattacherjee, A.S. Basavaraj, A.V. Rahul, M. Santhanam, R. Gettu, B. Panda, et al., Sustainable materials for 3D concrete printing, Cem. Concr. Compos. 122 (2021), 104156, https://doi.org/10.1016/J.CEMCONCOMP.2021.104156.
[41] Y. Chen, S. He, Y. Zhang, Z. Wan, O. Çopuroğlu, E. Schlangen, 3D printing of calcined clay-limestone-based cementitious materials, Cement Concr. Res. 149 (2021), 106553, https://doi.org/10.1016/J.CEMCONRES.2021.106553.
[42] C. Gosselin, R. Duballet, P. Roux, N. Gaudillière, J. Dirrenberger, P. Morel, Large-scale 3D printing of ultra-high performance concrete – a new processing route for architects and builders, Mater. Des. 100 (2016) 102–109, https://doi.org/10.1016/J.MATDES.2016.03.097.
[43] A. Perrot, A. Pierre, V.N. Nerella, R.J.M. Wolfs, E. Keita, S.A.O. Nair, et al., From analytical methods to numerical simulations: a process engineering toolbox for 3D concrete printing, Cem. Concr. Compos. 122 (2021), 104164, https://doi.org/10.1016/J.CEMCONCOMP.2021.104164.
[44] M. Moini, J. Olek, J.P. Youngblood, B. Magee, P.D. Zavattieri, Additive manufacturing and performance of architectured cement-based materials, Adv. Mater. 30 (2018), https://doi.org/10.1002/adma.201802123.
[45] Y.W.D. Tay, Y. Qian, M.J. Tan, Printability region for 3D concrete printing using slump and slump flow test, Composites, Part B 174 (2019), 106968, https://doi.org/10.1016/J.COMPOSITESB.2019.106968.
[46] Z. Chang, M. Liang, Y. Xu, Z. Wan, E. Schlangen, B. Šavija, Early-age creep of 3D printable mortar: experiments and analytical modelling, Cem. Concr. Compos. 138 (2023), https://doi.org/10.1016/J.CEMCONCOMP.2023.104973.
[47] Y. Chen, S.C. Figueiredo, Ç. Yalçinkaya, O. Çopuroğlu, F. Veer, E. Schlangen, The effect of viscosity-modifying admixture on the extrudability of limestone and calcined clay-based cementitious material for extrusion-based 3D concrete printing, Materials 12 (2019) 1374, https://doi.org/10.3390/MA12091374, 2019; 12:1374.
[48] S. Hou, Z. Duan, J. Xiao, J. Ye, A review of 3D printed concrete: performance requirements, testing measurements and mix design, Construct. Build. Mater. 273 (2021), 121745, https://doi.org/10.1016/J.CONBUILDMAT.2020.121745.
[49] A.L. van Overmeir, S.C. Figueiredo, B. Šavija, F.P. Bos, E. Schlangen, Design and analyses of printable strain hardening cementitious composites with optimized particle size distribution, Construct. Build. Mater. 324 (2022), 126411, https://doi.org/10.1016/J.CONBUILDMAT.2022.126411.
[50] Y. Chen, M. Liang, Y. Zhang, Z. Li, B. Šavija, E. Schlangen, et al., Can superabsorbent polymers be used as rheology modifiers for cementitious materials in the context of 3D concrete printing? Construct. Build. Mater. 371 (2023), 130777 https://doi.org/10.1016/J.CONBUILDMAT.2023.130777.
[51] F. De Larrard, C.F. Ferraris, T. Sedran, Fresh concrete: a Herschel-Bulkley material, Mater. Struct. Construct. 31 (1996) 494–498, https://doi.org/10.1007/bf02480474.
[52] I. Ivanova, V. Mechtcherine, Possibilities and challenges of constant shear rate test for evaluation of structural build-up rate of cementitious materials, Cement Concr. Res. 130 (2020), 105974, https://doi.org/10.1016/j.cemconres.2020.105974.
[53] C.D. Murray, The physiological principle of minimum work, Proc. Natl. Acad. Sci. USA 12 (1926) 207–214, https://doi.org/10.1073/pnas.12.3.207.
[54] B. Park, Y.C. Choi, Quantitative evaluation of crack self-healing in cement-based materials by absorption test, Construct. Build. Mater. 184 (2018) 1–10, https://doi.org/10.1016/j.conbuildmat.2018.06.206.
[55] Y. Chen, O. Çopuroğlu, C. Romero Rodriguez, FF.d. Mendonca Filho, E. Schlangen, Characterization of air-void systems in 3D printed cementitious materials using optical image scanning and X-ray computed tomography, Mater. Char. (2021) 173, https://doi.org/10.1016/j.matchar.2021.110948.
[56] Zhi, Wan;Yu, Zhang; Xu, Yading; Šavija B. Self-healing cementitious composites with a hollow vascular network created using 3D-printed sacrificial templates. Eng. Struct. n.d.:under review..